Title

Numerical Analysis of Experiments on Thermally Induced Dissociation of Methane Hydrates in Porous Media

Journal

Industrial & Engineering Chemistry Research, 57(17)

ISSN

0888-5885

Authors

Yin, Zhenyuan
Moridis, George
Chong, Zheng Rong
et al.

Publication Date

2018-05-02

DOI

10.1021/acs.iecr.7b03256

Peer reviewed

Numerical Analysis of Experiments on Thermally Induced Dissociation of Methane Hydrates in Porous Media

Zhenyuan Yin[†‡], George Moridis*[†‖⊥], Zheng Rong Chong[†], Hoon Kiang Tan[‡], and Praveen Linga*[†]

[†] Department of Chemical and Biomolecular Engineering, National University of Singapore, Singapore, 117585

[‡] Lloyd's Register Global Technology Centre Pte Ltd, Singapore, 138522

[‖] Petroleum Engineering Department, Texas A&M University, College Station, Texas 77843, United States

[⊥] Earth Sciences Division, Lawrence Berkeley National Laboratory, Berkeley, California 94720, United States

*E-mail: praveen.linga@nus.edu.sg., *E-mail: gjmoridis@lbl.gov.

Abstract

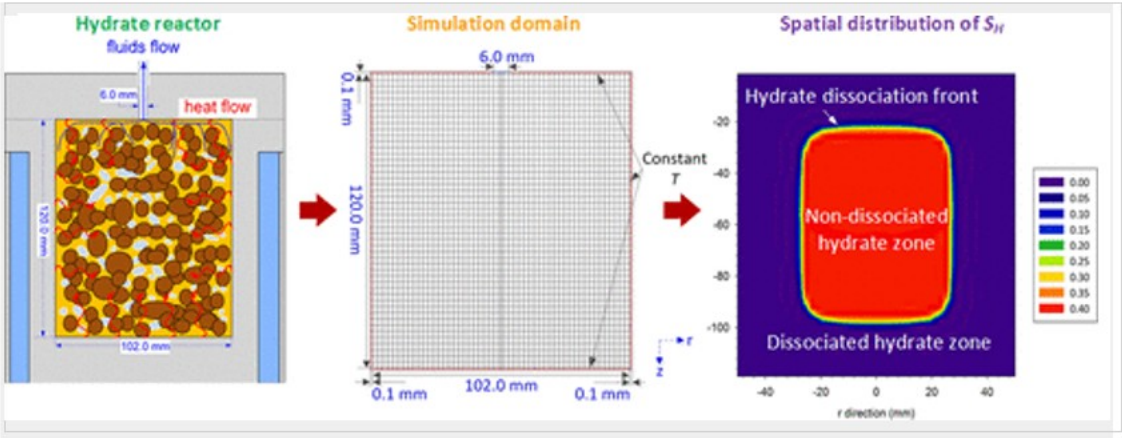

Numerical simulation is essential for the prediction and evaluation of hydrocarbon reservoir performance. Numerical simulators developed for the description of the behavior of hydrates under production and the corresponding flow of fluids and heat accounting for all known processes are powerful, but they need validation through comparison to field or experimental data in order to instill confidence in their predictions. In this study, we analyze by means of numerical simulation the results of an experiment of methane hydrate dissociation by thermal stimulation in unconsolidated porous media heated through the vessel walls. The physics captured by the model include multicomponent heat and mass transfer, multiphase flow through porous media, and the phase behavior of the CH_4 + H_2O system involved in methane hydrate formation and dissociation. The set of governing equations consists of the mass and energy conservation equations coupled with constitutive relationships, i.e., the dissolution of gas in H_2O, relative permeability and capillary pressure models, composite thermal conductivity models, and methane hydrate phase equilibria. The

model geometry describes accurately the hydrate reactor used in a recent experimental study investigating methane hydrate dissociation behavior [Chong et. al. *Appl. Energy* 2016, *177*, 409–421]. The cumulative gas production is estimated and validated against three tests of experimental data involving different boundary temperatures, showing a good agreement between observations and numerical predictions. The predicted evolution of the spatial distributions of different phases over time shows that hydrate dissociation progresses inward from the reactor boundary to the center, methane gas accumulates to the top of the reactor because of buoyancy, and water migrates down to the bottom of the reactor because of gravity. A sharp hydrate dissociation front is predicted, and the estimated location of hydrate dissociation front suggests a linear relationship with the square root of time. A sensitivity analysis on the thermal conductivity of sand under fully saturated conditions is conducted to elucidate its effect on the gas production behavior. In addition, the energy efficiency ratio computed from the simulation of this boundary-wall heating technique varies from 14.0 to 16.2. Deviations between observations and predictions of the evolution of the temperature profile are attributed to initial heterogeneous distribution of the hydrate phase in the hydrate reactor.

1. Introduction

Natural gas hydrates (NGHs) are solid crystalline compounds that consist of water and natural gas molecules, where water molecules form cagelike crystal lattices encaging the natural gas molecules under low-temperature and high-pressure conditions. NGHs in nature are typically found under deep sea and permafrost locations.(2−4) Methane is the most common hydrate-forming gas in nature in overwhelming abundance. Because of their ability to store effectively large amounts of gas (1 m^3 of CH_4 hydrate can contain as much as 184 m^3 of CH_4 at STP(5)) and the estimates of enormous recoverable CH_4 volumes from them (~20 000 trillion cubic meters(6)), methane hydrate (MH) reservoirs have been considered to be the next major unconventional source of energy. This realization provided the impetus for significant multidisciplinary research efforts in several countries (e.g., Canada, China, Germany, Japan, India, Russia, South Korea, Singapore, U.K., United States, etc.). Comprehensive drilling, logging, and coring programs have been implemented during the past two decades to identify the locations of promising MH reservoirs (as production targets) and determine their properties.(7) Field-scale production tests have been conducted in both permafrost and marine deposits to assess the technical feasibility of recovering CH_4 from MH reservoirs.(8) In addition, because of the paucity of undisturbed cores of hydrate-bearing sediments (HBS), there is a large body of research carried out in laboratories worldwide to synthesize hydrate samples that are representative of naturally occurring HBS. Such samples are critically important in the effort to characterize their mechanical and thermophysical properties and to study their formation and dissociation behavior.(9,10)

MH reservoirs are typically classified into four main classes: (i) Class 1 accumulations are composed of a hydrate-bearing layer (HBL) with an underlying two-phase fluid zone of mobile gas and liquid water. (ii) Class 2 deposits comprise a HBL overlying a zone of mobile water. (iii) Class 3 accumulations are composed of a single HBL without existence of underlying zone of mobile fluids. (iv) Class 4 hydrates refer to the many oceanic, dispersed, low-saturated hydrate accumulations.(8) There are three main production methods: (i) depressurization, in which the pressure (P) is lowered below the hydrate equilibrium pressure (P_{eq}) at the prevailing temperature (T); (ii) thermal stimulation, in which T is raised above the hydrate equilibrium temperature (T_{eq}) at the prevailing P; and (iii) use of inhibitors (salts or alcohols), which shift the hydrate P_{eq}–T_{eq}equilibrium.(11) The fourth method involves the use of CO_2 (and possibly other gases, such as N_2) to replace CH_4 in hydrates. It was proposed by Ohgaki et al.(12) and has been tested both in laboratory experiments(13) and during the Ignik Sikumi field test.(14) It is also possible (and often advisible) to use combinations of the aforementioned production methods.

A number of reservoir simulations on gas production behavior via various production methods for different classes of MH reservoirs have been carried out. A comprehensive summary of the production performance and conclusions drawn from simulations was presented by Moridis et al.(3) It was found that Class 1 reservoirs are the most promising and desirable systems that require the least amount of energy to destabilize and release gas.(15,16) Gas production from Classes 2 and 3 may have significant potential depending on the flow properties of the hydrate reservoir and the initial thermodynamic state of the hydrate,(17−22) and such potential can be significantly augmented by the use of horizontal wells.(23) Class 4 hydrate accumulations do not appear to be economically viable for gas production because of their unbounded nature and dispersed occurrence.(24,25) In addition, compared to the thermal stimulation method, depressurization is a more effective and economically viable approach for most hydrate reservoirs.(17)

The main thermophysical processes involved in hydrate dissociation are (a) mass transfer with multiphase fluid flow in porous media; (b) heat transfer by convection and conduction; and (c) the chemical and thermodynamic changes associated with state changes of the CH_4 + H_2O system during the reaction of hydrate dissociation and formation, including the associated enthalpy.(26)The three thermo-physical processes are coupled during hydrate dissociation–formation, and any one of them could become a limiting factor, depending on the dissociation methods and reservoir conditions. The hydrate formation–dissociation can be treated either as an equilibrium phenomena (appropriate for longer processes) or as a kinetic (appropriate for short-term processes) reaction.(23) Three classic kinetic models describing the kinetic behavior of CH_4 hydrate dissociation reviewed in the

literature(26) are (a) the Kim–Bishnoi model,(27) (b) the Selim–Sloan model,(28)and (c) the Yousif model.(29)

The Kim et al.(27) semiempirical model is based on fugacity differences (between the actual and the equilibrium conditions) being the driving force and assumes practically negligible heat- and mass-transfer resistance. Clarke and Bishnoi(30) further improved on the value of the intrinsic kinetic rate coefficient of the Kim–Bishnoi model by quantifying the hydrate particle size and the reaction surface area. The Kim–Bishnoi model has been widely adopted by most researchers quantifying the hydrate dissociation kinetic rate. The model of Selim and Sloan(28) treated hydrate dissociation as a one-dimensional (1D) semi-infinite moving-boundary ablation problem and involved an estimate of the moving speed of the hydrate dissociation front based on heat transfer under conditions of a constant boundary temperature(28) and a constant heat flux.(31) Scaling analysis of the governing equations led to the development of an analytical solution to the dissociation problem. The model of Yousif et al.(29) coupled multiphase flow behavior in porous media with a kinetic reaction of hydrate decomposition and formed a basis for hydrate reservoir modeling. The aforementioned 1D analytical models developed in the early 1990s were the underlying blocks for the 2D or 3D numerical models and reservoir simulators(32−34) developed later.

State-of-the-art hydrate reservoir simulators summarized in a review paper(26) include (a) the TOUGH+Hydrate simulator(35,36) and its earlier versions,(37−41) including the open-source version HydrateResSim;(42) (b) the MH21 code developed by a Japanese research team;(43) (c) the STOMP-HYD code developed by Pacific Northwest National Laboratory;(44) (d) the commercial simulator CMG-STARS developed by Computer Modeling Group;(45) and (e) the Hydrasim simulator developed by the University of Calgary.(46) Comparisons of several different reservoir simulation codes and their results using a set of test problems have been carried out and reported in several works.(47)

The application of numerical simulators to model hydrate dissociation behavior in laboratory-scale reactors provides unique opportunities for model validation under controlled conditions (a very difficult proposition under field conditions). Once this is achieved, a deeper understanding of the system behavior and the dominant factors controlling it can be gained, and the simulator can be used for better design of laboratory experiments.(48,49) For these reasons, such a use of numerical simulators is an important issue in the analysis of the significant body of research carried out in several laboratories around the world that focus on the formation and dissociation of hydrates and the corresponding gas and water production.(50−52) The scale of hydrate reactors typically varies from millimeters to meters,(9,51,52) which is substantially different from reservoir-scale studies that range from tens to hundreds or even thousands of meters.(38) Thus, the dissociation behavior (as affected by heat-transfer issues) and the rates of fluid (gas and

water) production are expected to be different depending on the scale of the study.

An understanding of the fundamentals of the hydrate dissociation behavior in laboratory experiments is important, as it can lead to the identification of important factors that control the system behavior. Such knowledge may be critically useful in the design and analysis of full-scale, long-term field tests of gas production from hydrates. Therefore, building confidence in the numerical models based on a good agreement between experimental data and numerical predictions is essential to bridge knowledge gaps and improve our understanding of the complex behavior of gas hydrates. A significant advantage of numerical simulation is its capability to provide relatively inexpensively (as compared to experiments) insights into the hydrate dissociation process, to identify key properties and parameters of the system, to assess production sensitivity to them, and to predict the flows of water and gas in the reservoir and to the wellbore under different scenarios. In addition, simulations can predict the evolution of the spatial distributions of the aqueous (A), gas (G), and hydrate (H) phases during the dissociation process. A number of flow, thermal, and thermodynamic properties (e.g., media porosity, permeability, thermal conductivity, specific heat, enthalpy of dissociation, kinetic reaction parameters, etc.) play a significant role in controlling hydrate dissociation through the interaction of the various coupled processes. Thus, multiple parametric studies and sensitivity analysis using numerical simulation can be conducted (often concurrently) to determine the relative importance of critical parameters and, consequently, to devise effective production strategies accordingly. Furthermore, numerical simulation used in an inverse modeling (history-matching) mode makes possible the estimation of key parameters and the optimization of production to meet specific criteria. A satisfactory match between observations and predictions through the optimization process can help validate the underlying constitutive models and the values of the associated parameters. (53,54)

The main objectives of this study are (a) to employ the state-of-the-art TOUGH+Hydrate v1.5 numerical simulator(35,36) (hereafter referred to as T+H) to investigate the dissociation of methane hydrates by thermal stimulation and the corresponding production of gas and water by analyzing data obtained from a set of earlier laboratory experiments involving a reactor heated through its boundary walls,(1) (b) to estimate critical system parameters through experimental measurements and a history-matching process that minimizes deviations between the model predictions and the laboratory measurements (thus contributing to the further validation of the T+H simulator), and (c) to identify the reasons for the remaining deviations between observations and predictions that cannot be further mitigated through the history-matching process. The various experimental data sets (obtained for different boundary temperatures) provide the necessary information for a robust evaluation of the dominant processes and of the

relevant parameters and for clearly determining trends associated with the thermally induced hydrate dissociation.

As a result of the simulation process, we also obtain the spatial distributions of the hydrate and gas-phase saturations at select times during the dissociation process. The investigation also includes (a) a sensitivity study on the composite thermal conductivity of the medium to assess its effect on dissociation and gas production, (b) a thermal analysis to evaluate the energy efficiency ratio (EER) of the thermally induced production method used in the laboratory experiments, and (c) a discussion of the possible effects of the assumption of uniformity in the initial hydrate saturation on fluids production.

2. Numerical Simulation

2.1. T+H Numerical Model

The simulations in this study were conducted using the T+H code,(35,36) a numerical simulator developed at the Lawrence Berkeley National Laboratory (LBNL) to model the nonisothermal behavior of CH_4 hydrate phase change (ΔH^0 measured to be 56.4 kJ/mol(55)), CH_4 release, and fluids flow under conditions typical of CH_4-hydrate deposits (i.e., in the permafrost and in deep ocean sediments, as well in any laboratory experimental setup) by solving the coupled equations of mass and energy balance equations associated with such systems. The code is written in standard FORTRAN 95/2003 to take advantage of all the object-oriented capabilities and the enhanced computational features of that language. It can model all the known processes involved in the system response of natural CH_4-hydrates in complex geologic media, including the flow of fluids and heat, the thermophysical properties of reservoir fluids, thermodynamic changes and phase behavior, and the nonisothermal chemical reaction of CH_4-hydrate formation and/or dissociation, which can be described by either an equilibrium or a kinetic model. T+H is a fully implicit compositional simulator, and its formulation accounts for heat and the various mass components that are partitioned among four possible phases: gas, aqueous liquid, ice, and hydrate. The T+H code can describe all the 15 possible thermodynamic states (phase combinations) of the CH_4+H_2O system (see Figure 1) and any combination of the three main hydrate dissociation methods: depressurization, thermal stimulation, and the effect of inhibitors. It can handle the phase changes, state transitions, strong nonlinearities, and steep solution surfaces that are typical of hydrate dissociation problems. A detailed description of the code, its underlying physics and capabilities, of the numerical techniques, and of the various options it provides can be found in the code's user's manual.(35) When hydrate formation–dissociation is treated as a kinetic reaction, the maximum number of mass components is four, i.e., H_2O, CH_4, CH_4-hydrate, and a water-soluble inhibitor such as a salt or an alcohol. For an equilibrium reaction, the CH_4-hydrate is not considered a separate chemical compound (component) but only a state of the H_2O–

CH_4system, and consequently, the maximum number of mass components is three: H_2O, CH_4, and a water-soluble inhibitor. Obviously, the kinetic model is computationally more demanding as it involves consideration of an additional mass balance equation per element of the discretized domain.

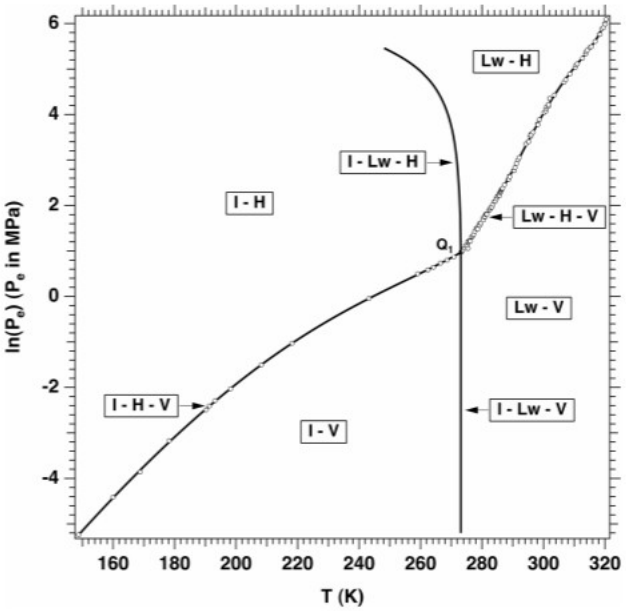

Figure 1. Pressure–temperature equilibrium relationship in the phase diagram of the CH_4 + H_2O + hydrate system in T+H showing all possible thermodynamic states.(35)

We modeled the methane hydrate dissociation induced by thermal stimulation caused by heating through the rector walls (boundary). In the laboratory experiments, the boundary wall had been kept at three different temperatures. Earlier studies(23,56) indicated that the treatment of dissociation as an equilibrium reaction is appropriate in long-term processes (such as gas production from hydrate deposits over long periods) and when the *P*- or *T*-anomaly that causes dissociation is significant, while a kinetic consideration is better suited to short-term processes (not exceeding a few days) and mild dissociation-inducing driving forces. An equilibrium reaction model is based on the assumption that CH_4-hydrate dissociation is fully controlled by the hydrate equilibrium curve, while a kinetic model employs the model of Kim et al.(27) to depict the hydrate dissociation rate. When the kinetic rate constant is large enough, a kinetic rate model would approach an equilibrium model. In addition, it was showed from a molecular dynamic study(57)that the CH_4-hydrate decomposition rate in a silica–water–hydrate system is much faster than in a hydrate–water system. For these reasons, and given the fact that the dissociation-inducing boundary temperatures in the study were considerably higher than those of the hydrate in the reactor (thus creating a strong driving force), we made the hypothesis that dissociation in a sandy medium could be treated as an equilibrium reaction in this numerical study despite the relatively short duration of the study. With the assumption of an equilibrium model, it is almost certain that this

will imply the fastest hydrate dissociation rate without kinetic retardation and the final CH_4recovery ratio will not be affected under the same outlet pressure. The P_{eq}–T_{eq} relationships in T+H that describe the liquid–hydrate–vapor (L–H–V) and the ice–hydrate–vapor (I–H–V) three-phase lines (states) at equilibrium during dissociation are shown in Figure 2.

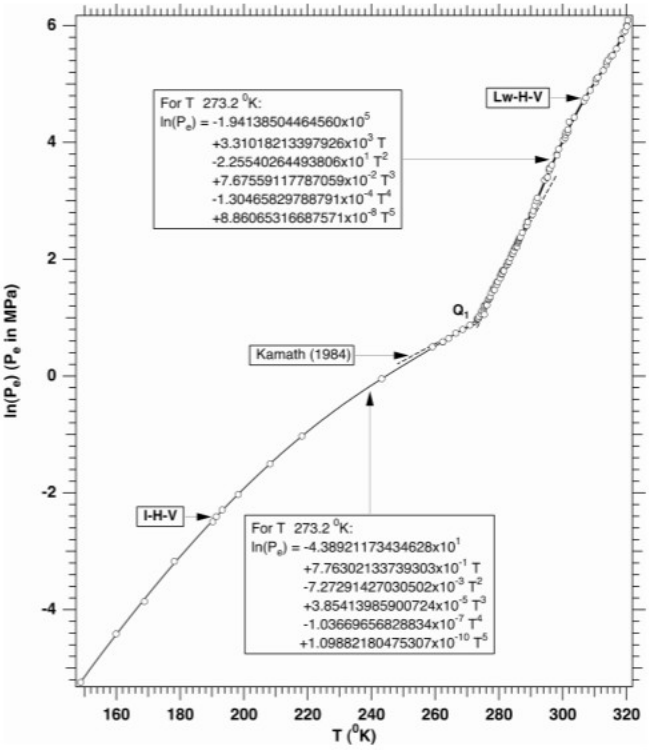

Figure 2. CH4-hydrate: relationship of the equilibrium hydration pressure Peq to the temperature Teq. (38)

2.2. Model Geometry and Domain Discretization

The simulation domain is depicted in Figure 3 and accurately represented the hydrate reactor, which is shown in the photograph (Figure S1) and in the cross-sectional schematic drawing (Figure 4). The detailed dimension of the cylindrical hydrate reactor is summarized in Table 1. A schematic of the complete apparatus used in the laboratory experiments simulating hydrate formation and dissociation is shown in Figure S2.

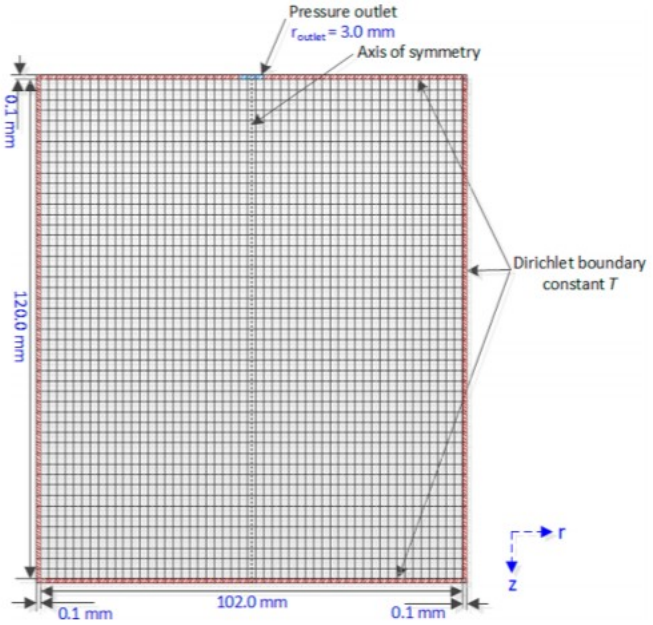

Figure 3. Simulation domain describing the hydrate reactor employed in the experimental study.

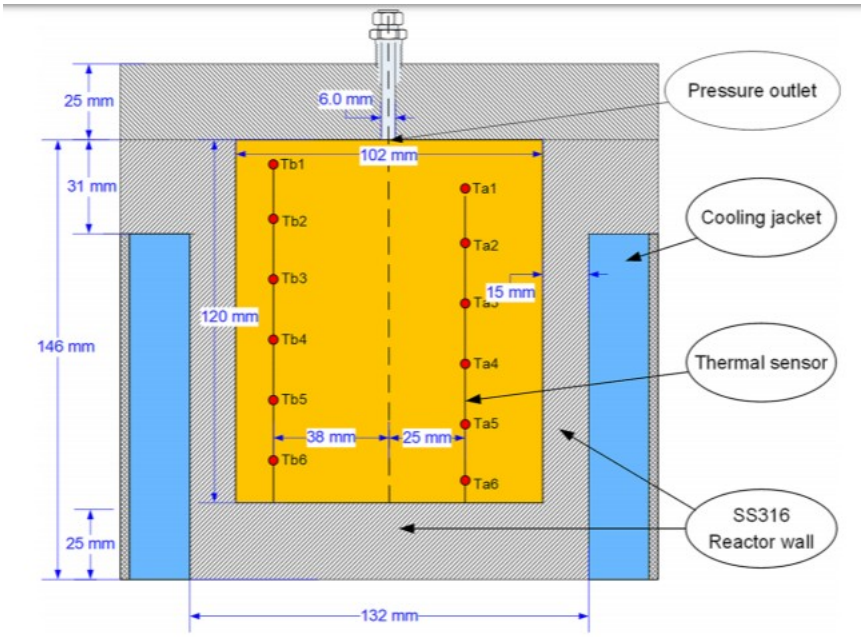

Figure 4. Cross-sectional view of the hydrate reactor confirming the accuracy of the simulation domain (shaded in orange) in Figure 3.

Table 1. Geometry of the Hydrate Reactor and Pressure Outlet

Parameter	value
internal height of reactor	120.0 mm

Parameter	value
internal diameter of reactor	102.0 mm
internal volume of reactor	0.98 SL
thickness of reactor wall	15.0 mm
thickness of reactor top and bottom	25.0 mm
external diameter of pressure outlet	10.00 mm
internal diameter of pressure outlet	6.00 mm
material of reactor	SS316

Because of radial symmetry, the domain is represented by a cylindrical axisymmetric system. We used the MeshMaker v1.5 application(58) for the creation of the simulation mesh. The radius of the hydrate reactor is discretized into 26 subdivisions Δr (1 × 1.0 mm and 25 × 2.0 mm), with an additional outermost element (cell) of Δr = 0.1 mm at the outer rim of the domain representing the constant-temperature boundary where the circulating water bath is located. The height of the interior of the reactor is discretized into 48 subdivisions of equal size Δz = 2.5 mm, with 2 additional elements of size Δz = 0.1 mm at the top and bottom of the system representing the constant-temperature boundaries of the domain. The pressure outlet is located at the top center of the apparatus and has a radius of 3.0 mm in Figure 3. This discretization resulted in a total of 1350 cells. Of these, 1248 were active cells depicting the reactor core with the dissociating hydrate and 102 were inactive cells representing the time-invariable boundaries. The equilibrium dissociation option chosen to analyze the results of the laboratory study involved the solution of 3 equations per element (the mass balance of the H_2O and the CH_4 components and the heat balance of the entire system), resulting in a system of 3744 simultaneous equations.

2.3. Initial and Boundary Conditions

The initial conditions (P, T, and phase saturations) in the hydrate-bearing sand in the reactor core were estimated from experimental measurement(1) and are listed in Table 2. The phase saturations are assumed to be uniformly distributed in the system and are the same for all experiments and simulation cases. Similarly, the flow properties (porosity and permeability; see Table S1) were assumed to be homogeneous and isotropic in the core. It is important to note that the assumption of uniform spatial distributions of the various phase (a) may have important implications in the analysis of the experimental results and (b) could not be independently validated through direct observations because of lack of X-ray computed tomography (CT) scanning facilities, but (c) it is possible (but by no means certain) that information on its validity could be inferred from the simulation results.

Table 2. Initial Conditions of Hydrate Bearing Sediment Inside Hydrate Reactor

parameter	value
gas composition	100% CH_4
initial pressure	6.2 MPa
initial temperature	281.5 K
bottom hole pressure	4.5 MPa
initial hydrate saturation (S_H)	0.4
initial aqueous saturation (S_A)	0.56
initial gas saturation (S_G)	0.04
hydration number (N_H)	6.1

The specifics of the three laboratory experiments of hydrate dissociation by thermal stimulation (labeled as H3, H5, and H6, as was the naming convention in the experimental study(1)) are listed in Table 3, which

corresponds to simulation cases (cases 1, 2, and 3, respectively). In addition, two simulation cases associated with the conditions of the H2 experiment (cases 4 and 5) are listed that aim to determine the system sensitivity and response to the thermal conductivity of the porous medium under fully saturated conditions (referred to as “wet” thermal conductivity).

Table 3. Boundary Conditions and Sand Wet Thermal Conductivities in Simulated Cases

dissociation method	experiment/ simulation cases	outlet pressure (MPa)	boundary temperature (K)	sand wet thermal conductivity (W/m/K)
thermal stimulation	H3/case 1	4.5	280.7	0.5
	H5/case 2	4.5	283.2	0.5
	H6/case 3	4.5	285.2	0.5
	H5/case 4	4.5	283.2	1.5
	H5/case 5	4.5	283.2	2.5

The outermost subdivisions of the discretized domain (at the top, bottom, and maximum radius of the domain) surround the representation of the reactor core and describe the circulating water bath that was kept at constant temperatures (i.e., they are Dirichlet-type boundaries) that are sufficiently high to induce hydrate dissociation in the various experiments. The three experiments and the corresponding simulation cases differed from each other only in the boundary temperatures of the circulating water. Table 3 also lists the boundary temperatures in the various experiments and cases, as well as the $k_{\theta w}$ values used in the simulations. Figure 5 shows a schematic of the initial state (defined by its location in the CH_4–H_2O phase diagram) of the hydrate in the reactor prior to the dissociation, as well as the final states in the three experiments. Note that in all cases the pressure and temperature were set above the quadruple point of CH_4-hydrate to prevent the formation of ice.

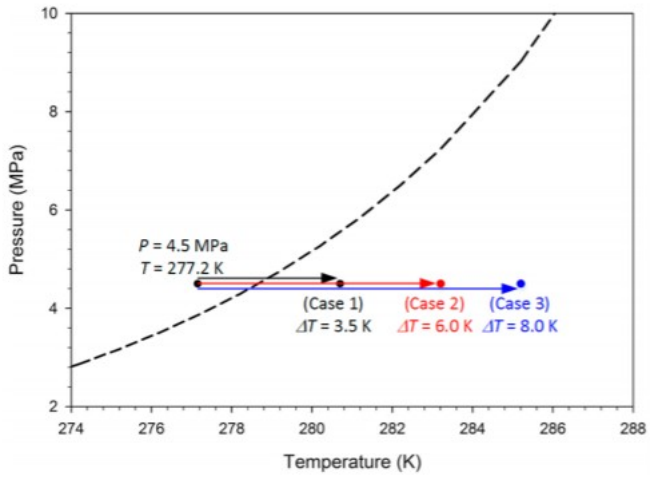

Figure 5. Initial condition and boundary conditions in cases 1, 2, and 3 in relation to CH_4-hydrate P_{eq}–T_{eq}.

2.4. Determination of the Properties of the Porous Medium

The properties of the porous medium and of the CH_4-hydrate are critical input parameters in the numerical model. The porosity, ϕ, and the absolute permeability, k, of the porous media affect the fluid flow behavior, which in turn determines the gas and water production rates. Even more importantly, the thermal properties (i.e., the composite thermal conductivity, k_θ, and specific heat, C_R, of the hydrate-impregnated sand) play a critical role in the thermally induced dissociation of hydrates (and fluid production) in this study because they control the heat transfer from the boundaries to support the endothermic dissociation reaction.

The porous medium used in this study was unconsolidated filter sand (type W9, supplied by River Sands Pte Ltd.) with a quartz content exceeding 99%. The values of the flow and thermal properties of the system components were measured directly in appropriate experiments in this work, thus obtaining accurate data and reducing uncertainties that would have complicated the analysis of the laboratory results. Mercury porosimetry test on sand samples had determined that $\phi = 0.44$ and $k = 3.83$ Darcy. The grain density was measured as $\rho = 2650$ kg/m^3; the sand had an average grain size of 212.0 µm and an average pore diameter of 21.8 µm. The fluid relative permeabilities and the capillary pressure are described by the modified Stone's model(59) and van Genucheten model(60,61) with parameters listed in Table S1 from history-matching techniques and are shown in Figures S3 and S4, respectively.

Using a differential scanning calorimetry test, we estimated the specific heat of the sand as $C_R = 800$ J/kg/K. From the stoichiometry of the CH_4-hydrates and basic mass balance equations, the initial saturation of the hydrate in the reactor was estimated as $S_H = 40\%$, and the aqueous and gas-phase saturations were $S_A = 50\%$ and $S_G = 10\%$, respectively.(1) The physical properties of the porous media and of the hydrates, as well as important

constitutive equations describing the behavior of the hydrate-bearing system, are summarized in Table S1. All the thermophysical properties of the water, of the gas, and of the hydrate are provided by appropriate correlations that are available in the T+H codes.(35)

2.5. Monitored Variables and Parameters

As discussed earlier, the assumption of the dissociation reaction as an equilibrium process (for the reasons explained in section 2.1) leads to a matrix equation involving a total of 3744 algebraic equations that need to be solved at each Newtonian iteration (of the fully implicit method employed in T+H) and at each time step. The total simulation time in each case was set to 10 h, which was deemed sufficient to ensure complete hydrate dissociation and the attainment of a steady state.

In order to compare the numerical predictions of the cumulative gas production to the experimental data, we monitored (a) the cumulative gas production V_T through the pressure outlet of the experimental apparatus (accurately represented in the discretized domain), as well as (b) the pore volume-averaged properties and conditions (i.e., P, T, S_H, S_A, and S_G) of the reactor interior and at specific locations. It is important to note that the heat exchange between the reactor and its surrounding (the outer boundary of the system) was fully accounted for, allowing estimation of the associated energy consumption and the energy efficiency ratio.(31,62)

3. Results and Discussion

We simulated three cases (cases 1, 2, and 3) of hydrate dissociation by thermal stimulation induced by three different temperature differentials (ΔT = 3.5, 6.0, and 8.0 K; see Table 3). The results of the simulation are evaluated through comparison of the experimental data to the predictions of the following variables: (1) V_T; (2) T; (3) the evolution of S_H and S_G; and (4) the location of the hydrate dissociation front, $X(t)$. In this work, the hydrate dissociation front is described by the location where S_H begins to fall below its initial level. Case 2 (ΔT = 6.0 K) is selected as the reference case. Cases 2, 4, and 5 differ only in the “wet thermal conductivity ($k_{\theta w}$)” values of the sand, which are 0.5, 1.5, and 2.5 W/m/K, respectively. The $k_{\theta w}$ value of 2.5 W/m/K for quartz sand was estimated from a geometric mean model proposed by Cote and Konrad(63)with ϕ = 0.44 in our quartz sandy medium. The values of 0.5 and 1.5 W/m/K were also reported in other sandy medium with different grain size and sorting(64−66) and are within (although on the low end of) the range for sandy porous media.

3.1. Cumulative Gas Production (V_T) and Comparison with Experimental Data

Figure 6 shows the experimental data (round dots) and the numerical predictions (solid lines) of $V_T$during dissociation. The agreement between the two sets of data is good; the average deviations between the two sets are 5.8%, 4.8%, and 3.7% in cases 1, 2, and 3, respectively. We calculated the average rate of gas production during the initial 2 h (Q_{2h}) and estimated the

time needed for 50% of the hydrate mass to dissociate ($t_{1/2}$). A comparison of the V_T, Q_{2h}, and $t_{1/2}$ data between the simulation and experimental results is summarized in Table 4. As expected, $t_{1/2}$ decreases as the boundary temperature increases in both the simulation and the experiment results. V_T in the simulation study is estimated to be 22.84 L in case 2, which is in good agreement with the experimental average value of 23.86 L in H5 (exhibiting a deviation of 4.4%).

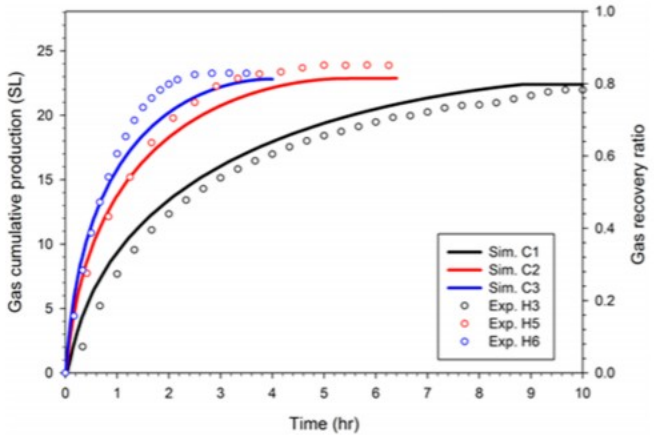

Figure 6. Cumulative gas production (V_T) profiles comparison between simulation predictions (cases 1, 2, and 3) and experimental measurements (H3, H5, and H6).

Table 4. Comparison of V_T, $t_{1/2}$, and Q_{2h} between Simulation Prediction and Experimental Observation

simulation study (this work)				experimental study(1)			
simulation case	V_T(SL)	$t_{1/2}$(hr)	R_{2h}(L/h)	experimental case	V_T(SL)	$t_{1/2}$(hr)	R_{2h}(L/h)
case 1	22.40	1.39	6.70	H3	23.26	1.79	6.20
case 2 (base case)	22.84	0.69	9.13	H5	23.86	0.89	9.45
case 3	22.92	0.42	10.55	H6	23.28	0.54	11.08
case 4	22.51	0.25	19.97[a]				

simulation study (this work)				experimental study(1)			
simulation case	V_T(SL)	$t_{1/2}$(hr)	R_{2h}(L/h)	experimental case	V_T(SL)	$t_{1/2}$(hr)	R_{2h}(L/h)
case 5	22.51	0.16	22.05[a]				

[a] First hour cumulative gas production rate are reported in cases 4 and 5 because dissociation completes within 2 h.

The simulation study generally predicts a faster hydrate dissociation rate and, consequently, a shorter $t_{1/2}$ and a faster Q_{2h} than the experiment. The faster dissociation is attributed to the following two factors: (a) the assumption of equilibrium dissociation and, to a lesser extent, (b) to the assumption of uniform hydrate distribution at the beginning of dissociation. Note that the numerical predictions indicate faster (than the experimental) dissociation despite the fact that the thermal conductivity values in this study (which is controlled by heat transfer rather than flow processes) are on the lower end of the spectrum. This tends to further support the conclusion that kinetic retardation is the reason for the experimental $t_{1/2}$.

On the basis of past experimental observations,(1) not all of the methane gas released from the complete hydrate dissociation is collected in the receiver because of the backpressure (P = 4.5 MPa) implemented. We employ the concept of *gas recovery ratio* (GRR) in order to assess the cumulative gas production from a reservoir engineering perspective. GRR is defined as the ratio of CH_4 recovered from the pressure outlet to the amount of CH_4 dissociated in the hydrate reactor. The initial amount of CH_4 in the reactor pore volume is 28.0 L (STP), as estimated by T+H. The final overall GRR values calculated from the simulation results are 80.0%, 81.6%, and 81.9%, corresponding to the increasing boundary temperatures in cases 1, 2, and 3, respectively. The GRR values estimated from the experimental results are 83.1%, 85.2%, and 83.1%. These values suggest that (a) there is a good agreement between the numerical simulation and the experimental results and (b) that the different boundary temperatures (280.7–285.2 K) have a limited effect on the GRR, which remains practically the same in all cases. This was expected because all the boundary temperatures are comfortably above the equilibrium dissociation temperature of the hydrate at the pressure of the experiment, which means that about the same amount of hydrate will be dissociated in all cases, with the only difference being the rate at which the dissociation proceeds. Thus, it can be expected that different temperatures applied at the boundary will not have a strong impact on the final GRR at the end of MH dissociation with the same backpressure in

a hydrate-bearing reactor if these temperatures are above the equilibrium temperature of hydrate dissociation at the reactor pressure. However, deviations may exist (and are normal and expected) from batch to batch in experiments because of inevitable differences in the packing of the sand, which may affect its porosity and its thermophysical properties.

3.2. Evolution of the Spatial Distribution of S_H, S_G, and S_A

A powerful feature of numerical simulation is its capability to help visualize the saturations of different phases inside the hydrate reactor. This capability can provide important insights on how hydrate, aqueous, and gas phases distribute and evolve during the hydrate dissociation process. Figure 7a–f shows the evolution of S_H inside the reactor at different times (from t = 10 min to t = 250 min). It can be seen that the dissociation of the hydrate core precedes both radially and vertically inside the cylindrical hydrate reactor once the boundary-wall temperature is increased. As expected, the dissociation progressed from the outer rim (where the higher-temperature boundary was located) toward the inner part of the core. The shape of the hydrate block is cylindrical at the beginning and continues to shrink while maintaining a symmetric (but increasingly ellipsoidal) shape as dissociation proceeds.

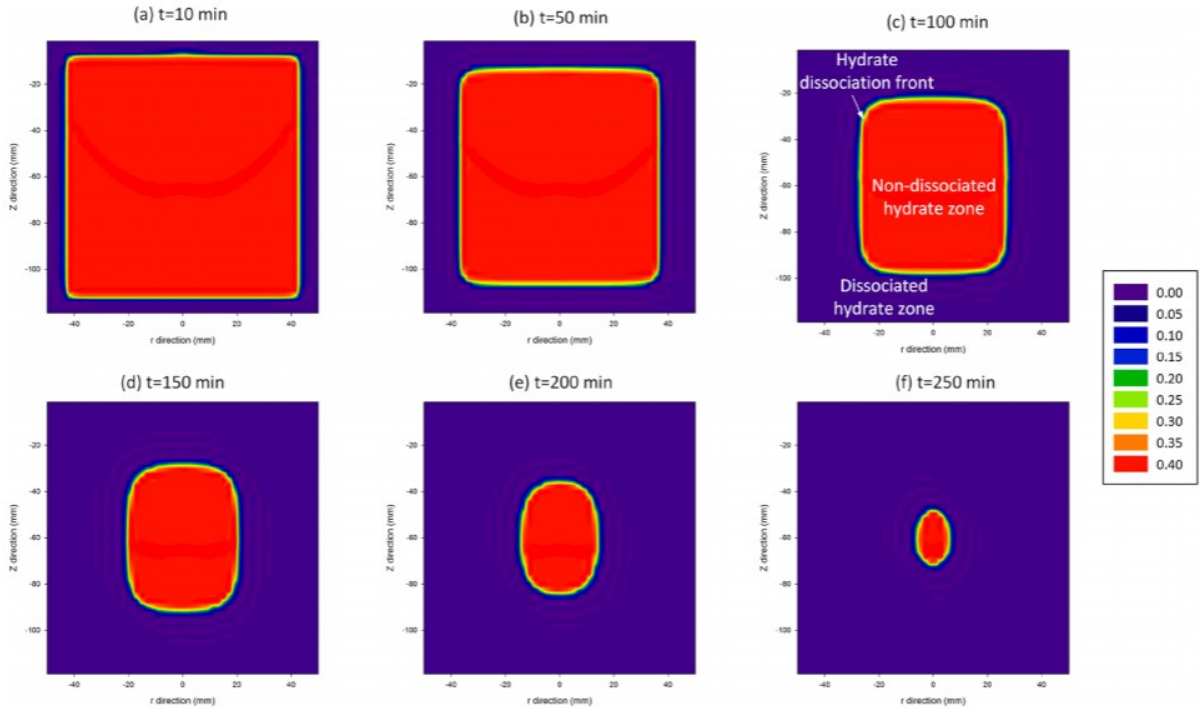

Figure 7. Evolution of S_H spatial distribution from (a) t = 10.0 min to (f) t = 250.0 min in case 2 with three zones identified shown in panel c (i.e., dissociated hydrate zone, nondissociated hydrate zone, and hydrate dissociation front).

Three different zones are identified at each time shown in Figure 7c: (a) the nondissociated hydrate zone, in which S_H is about 0.4 and remains practically constant; (b) a hydrate-free dissociated hydrate zone where its S_H = 0; and

(c) a sharp hydrate dissociation front where $S_H$decreases rapidly from 0.4 to 0. In the hydrate-free region, gas and water occupy the pore volume, and the spatial distributions of their saturations are expected to be heterogeneous and complex: methane gas will tend to rise and concentrate at the top because of buoyancy while water will likely concentrate at the bottom of the reactor because of gravity, but the gravitational effects on the S_A distributions will be mitigated to a certain degree because of capillary effects.

These expectations are confirmed in Figures 8a–f and 9a–f, which show the evolution of the spatial distribution of S_G (containing mostly CH_4) and S_A during hydrate dissociation from t = 10 min to t = 250 min. S_G is initially low and maintained at about the 10% level in the nondissociated hydrate zone inside the reactor. Reviewing S_G in the dissociated hydrate zone, as depicted in Figure 7a–c, the gas concentration is initially high at the hydrate dissociation front. Methane gas slowly migrates toward the upper section of the reactor because of buoyancy, where it accumulates, reaching a final saturation of about 75–80%. The gas released from the dissociating hydrate is discharged through the pressure outlet of the hydrate reactor, driven by the increasing Pin the reactor. Conversely, the water released from the hydrate dissociation moves downward because of gravity and accumulates at the bottom of the reactor as depicted in Figure 9a–c, where S_G decreases to 10–15% and S_A increase to 85–90%.

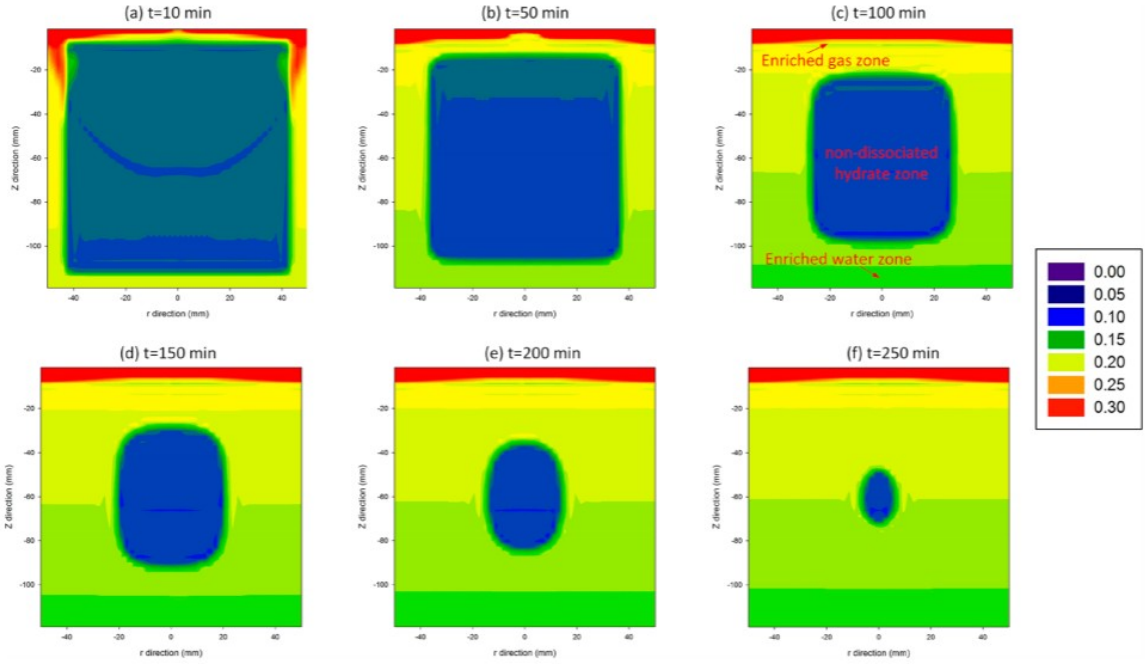

Figure 8. Evolution of S_G spatial distribution from (a) t = 10.0 min to (f) t = 250.0 min in case 2 with three zones identified shown in panel c (i.e., enriched gas zone, enriched water zone, and nondissociated hydrate zone).

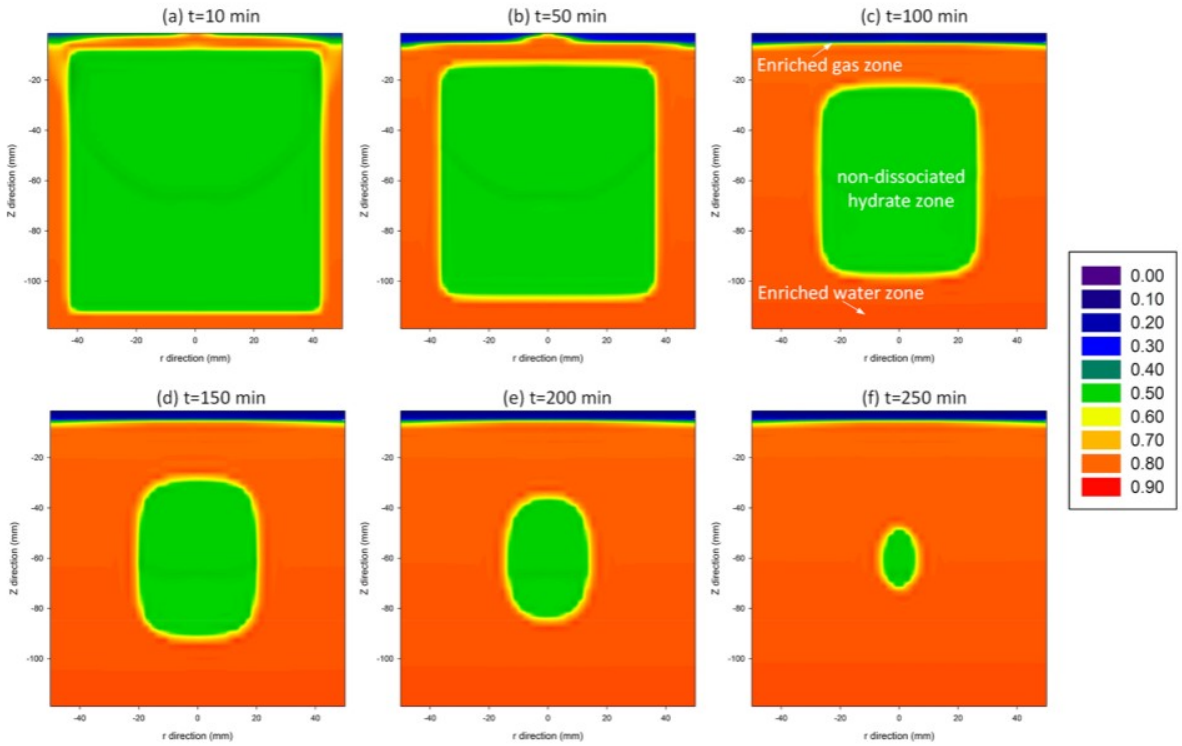

Figure 9. Evolution of S_A spatial distribution from (a) t = 10.0 min to (f) t = 250.0 min in case 2 with three zones identified shown in panel c (i.e., enriched gas zone, enriched water zone, and nondissociated hydrate zone).

A close examination on the inward advancement of the hydrate dissociation front along the radial direction, as estimated from the simulation study, indicates that this occurs at a decreasing rate of advance. Figure 10 shows a very strong linear correlation between the location of the advancing hydrate dissociation front $X(t)$ and $t^{1/2}$ for all cases (1 to 3). Correlation analysis yields the best linear fit lines as $X(t) = 5.31 \times 10^{-4}\ t^{1/2}$, $X(t) = 4.49 \times 10^{-4}\ t^{1/2}$, and $X(t) = 3.02 \times 10^{-4}\ t^{1/2}$ in cases 1, 2, and 3, respectively. The rate of advance of the hydrate dissociation front (represented by the gradient of the linear fit line) increases with an increasing boundary-wall temperature.

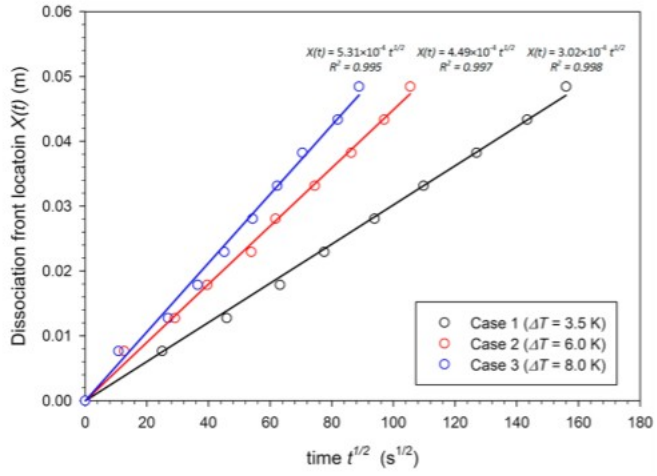

Figure 10. Location of hydrate dissociation front $X(t)$ against $t^{1/2}$ in cases 1, 2, and 3.

This linear relationship between hydrate dissociation front and time to the power of 1/2 is entirely analogous to the analytical model of Paterson(67,68) for heat-transfer and phase change (ice melting) problems in cylindrical domains, which is described as $X(t) = 2\xi(\alpha t)^{1/2}$. For a thermal diffusivity of methane hydrate $\alpha = 2.04 \times 10^{-7}$ m^2/s (as measured by Rosenbaum et al. (69)), the nondimensional parameter ξ is calculated as 1.02, 2.26, and 3.16 in cases 1, 2 and 3, respectively. Although ice melting and hydrate dissociation are different processes (because of the release of gas in the case of hydrates), there may exist sufficient similarity to allow the use of such an equation as an approximate tool for the estimation of the rate of advance of hydrate dissociation inside a reactor exposed to different boundary temperatures. A similar methodology has been applied in the numerical study of hydrate dissociation by depressurization.(70)

3.3. Evolution of the Spatial Distribution of T

Figure 11a–f shows numerical predictions of the evolution of the spatial distribution of T inside the hydrate reactor over time (from $t = 10$ min to $t = 250$ min) in case 2 ($\Delta T = 6.0$ K). Figure 12 shows the predicted phase saturations and T along the radial direction at $z = -60.1$ mm and at $t = 100$ min. It is obvious that the spatial distribution of T depends on the distribution of S_H and the loci of hydrate dissociation. A clear temperature difference exists between the nondissociated and the dissociated/dissociating hydrate zone. Within the nondissociated hydrate region, T is maintained at approximately 278.6 K (T_{eq} at the $P = 4.5$ MPa). Outside the hydrate region, T keeps increasing from T_{eq} to the boundary-wall temperature ($T = 283.2$ K). The heat flowing from the boundary wall into the reactor has to propagate through the sandy porous medium of the dissociated zone. This zone, the pore space of which is occupied by gas and water, and its expanding size decelerates the rate of advance of the dissociation front because heat flowing from the boundary wall has to cover an increasing distance to the hydrate. Note that there is a significant assumption underlying all the results discussed in Figures 6–12, namely, that the hydrate saturation at the beginning of the dissociation process is uniform in the entire reactor volume. This is a significant assumption that can significantly affect both the cumulative production results and the predictions of the spatial distributions of P, T, and phase saturations.

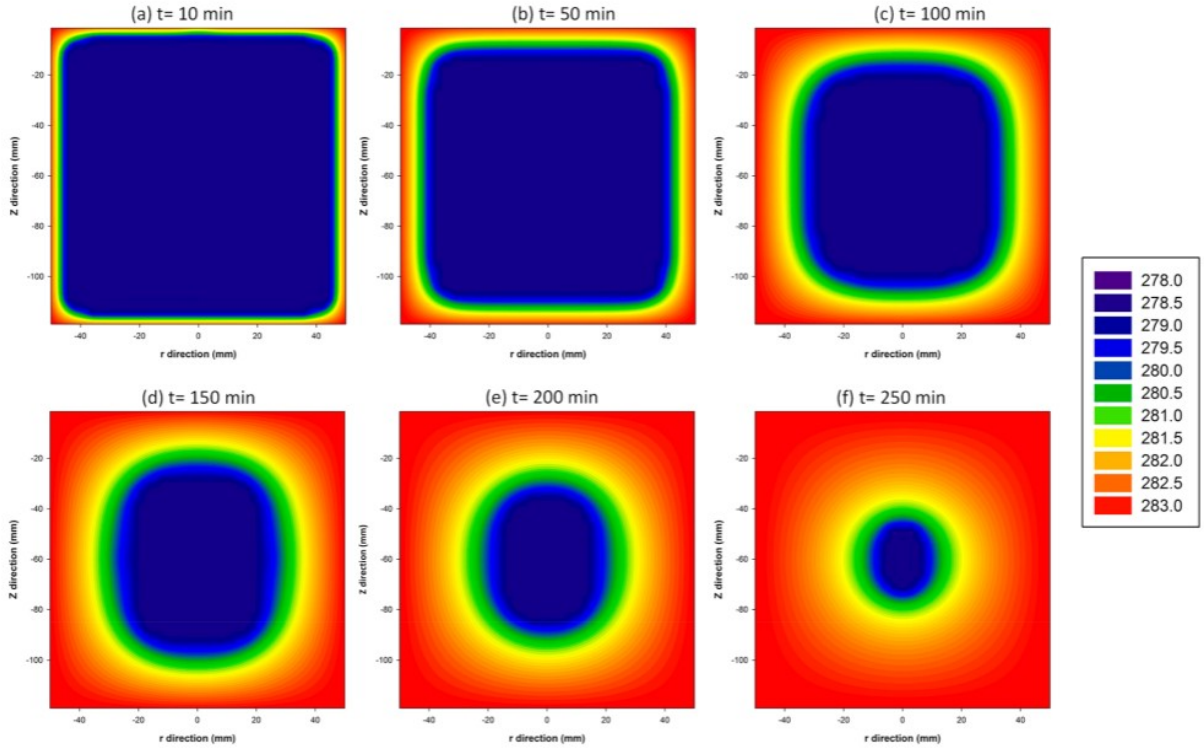

Figure 11. Evolution of T spatial distribution from (a) t = 10 min to (f) t = 250 min in case 2.

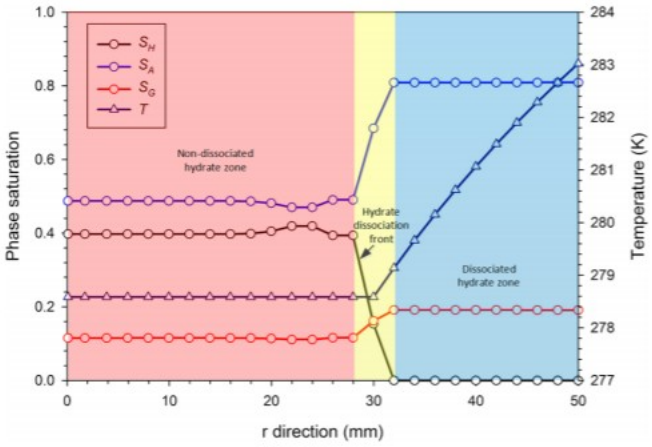

Figure 12. T, S_A, S_G, and S_H along radial direction at z = −60.0 mm for t = 100 min in case 2.

Figure 13 shows a comparison of the evolution of T obtained from the simulation results and from the experimental measurements at the two specific locations (T_{a4} and T_{b4}) shown in the included schematic. In the experimental study,(1) 12 thermal sensors were installed inside the hydrate reactor. Six of them were located at r = 25.0 mm from the center of the reactor, and the remaining six were located at r = 38.0 mm (Figure 4). The two locations indicated in the schematic in Figure 13 were part of the sensor array, and the numerical simulation study monitored the evolution of temperatures at these locations, which had been selected to be close to the center core of the reactor. It can be seen that the numerical predictions and

the experimental results show temperatures rising from its initial level of 277.2 K to the final temperature equal to that of the boundary wall (283.2 K) in about 4.0 h. As expected, the temperature rise at r = 25.0 mm lags behind that at r = 38.0 mm because of its greater distance from the constant-temperature boundary. This is observed in both the experimental study and in the numerical predictions, but the lag is far more pronounced in the numerical results. This significant delay is attributed not only to the greater distance from the boundary but also to the heterogeneity of the sand packing and of the hydrate saturation (neither of which could be determined without the use of CT scanning) and to the assumption of an equilibrium dissociation reaction that results in intense localized temperature variations that take time to propagate through the system.

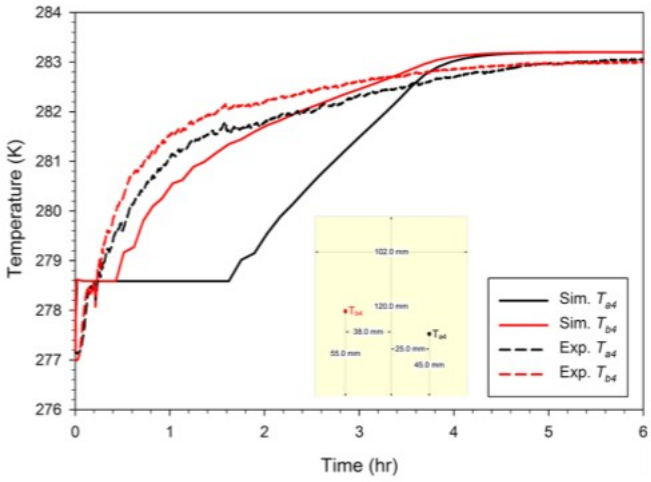

Figure 13. Evolution of T at T_{a4} and T_{b4} positions shown in schematic in case 2.

Expanding on this point, the significant deviation between the experimental measurements and the simulation results is the time at which T remains at the level of the hydrate equilibrium temperature (T = 278.6 K at the reactor pressure). The experimental data exhibit a short dip in temperature near the hydrate equilibrium temperature that lasts about 10 min. Conversely, the simulation results are characterized by a temperature that remains constant at the equilibrium level for about 1.8 h at T_{a4} (r = 25.0 mm) and 0.7 h at T_{b4} (r = 38.0 mm). To explain the deviation between the two results, three primary reasons are identified: (a) the heterogeneity in the initial hydrate saturation distribution inside the hydrate reactor; (b) uncertainty about the thermal properties of the sand–hydrate–fluid system, which had not been measured directly; and (c) the assumption of equilibrium (as opposed to kinetic) dissociation.

In the apparatus used for the experiments that are numerically analyzed in our study, the thermal stimulation is controlled by the temperature of the reactor boundary wall. Thus, it is almost certain hydrates would concentrate next to the reactor walls during hydrate formation or the bottom of the reactor, with S_H decreasing toward the center of the reactor. However, the

spatial distribution of $S_H$is also strongly dependent on the initial distribution of S_A and S_G (i.e., the location of the water injection, the duration for the water drainage) and the flow properties of the sandy medium (P_{cap}, S_{irw}, ϕ, and k). Upon dissociation, this initial S_H spatial distribution is expected to lead to a rapid dissociation near the reactor boundary, with the inner part responding later and slower (in terms of changing T). Thus, the heterogeneous distribution of the hydrate will significantly affect the Tdistribution, as the former affects both the location and the rate of the endothermic dissociation reaction, as well as the heat flow through the system.

As discussed earlier, the thermal conductivity of wet sand $k_{\theta w}$ in this study is 0.5 W/m/K. This is within the possible range for quartz sand but is close to the very low end of the range,(64,66) and there is no certainty that is an accurate estimate. Direct measurements are needed to provide accurate $k_{\theta w}$ inputs for the numerical model and thus reduce uncertainties and better quantify the composite thermal conductivity of hydrate-bearing sediment (k_θ),(54,71) the heat flow, and overall thermal behavior in the reactor. Finally, in the equilibrium model assumed in the simulations, hydrate dissociation occurs at equilibrium (P_{eq}–T_{eq}) conditions. In a kinetic model, hydrate dissociation is possible at nonequilibrium conditions and is characterized by a kinetic retardation that allows more time of heat propagation and lessening of the intense localizations of temperature associated with equilibrium dissociation. Thus, a kinetic model is likely to result in a more diffusive hydrate dissociation front and a much smoother shape of the T-distribution.(23)

In addition, the deviated evolution of T could also be attributed to the heat transport model, which may not adequately capture the pore-scale and microscale behavior during CH_4-hydrate dissociation. During a thermally induced CH_4-dissociation process with high water saturation (S_A > 50%), both direct dissociation as well as local rearrangements of nonuniform hydrates can happen in the pore space. Moreover, adsorbed layers on minerals at the surface of quartz sand are thin (1.5 nm roughly(72)) and very sensitive to heat. It was also shown from previous molecular dynamic studies(73−75) that nanobubbles tend to form under a fast CH_4 hydrate dissociation rate. Therefore, the whole dynamics of hydrate particles dissociation and the release of gas and bridging water between the mineral layer and hydrate are very complex. The heat transport problem is actually very geometry-dependent because hydrates will not be cementing, and the hydrate particle geometry will not follow the shape of the pore when diminishing. Thus, there is a strong need to observe these microscale and pore-scale behaviors during CH_4-hydrate formation and dissociation in laboratories and to further develop a more representative model accounting for these phenomena.

3.4. Sensitivity Analysis of the Effect of the Thermal Conductivity of Sand ($k_{\theta w}$)

In this study of thermally induced hydrate dissociation by means of heating through the system boundaries (the reactor walls, kept at constant temperatures), the limited potential for significant flow within the reactor indicates that the dissociation is likely to be controlled by thermal processes, leading to a belief that the thermal conductivity of the sand may have a major effect on the hydrate dissociation rate. To investigate this issue, we conducted a sensitivity analysis study involving three different $k_{\theta w}$ (0.5, 1.5, and 2.5 W/m/K in cases 2, 4 and 5, respectively; see Table 3). In all these the boundary temperature was the same as in the reference case 2 (ΔT = 6.0 K). The $k_{\theta w}$ values used in this study are within the range (but at the low end of it) reported in laboratory studies.(64) Note that it is important to conduct laboratory studies in order to develop reliable models describing the effects of the porosity and of the saturations of various phases on the composite $k_{\theta w}$ of porous media. Although the presence of various phases is known to have a significant impact on $k_{\theta w}$,(76) the subject is far from resolved, and more supporting studies are needed in order to quantify the problem.

Figure 14 shows V_T predicted in cases 2, 4, and 5. The total volume of produced gas (V_T) estimated in cases 4 and 5 is 22.51 L, indicating a gas recovery of 80.39%, which is close to the value of 81.6% in the reference case 2. The $t_{1/2}$ and Q_{2h} for cases 4 and 5 are also included in Table 4. From $t_{1/2}$ = 0.69 in case 2, $t_{1/2}$ declines significantly to 0.25 and 0.16 h with the increasing sand thermal conductivity in cases 4 and 5, respectively. In both cases 4 and 5, the time to complete hydrate dissociation is less than 2 h (see Figure 14). These results confirm expectations: because flow is limited and dissociation is controlled by conductive heat flows, the rate of hydrate dissociation and methane gas production increases with an increasing $k_{\theta w}$ when all other thermophysical properties are the same. Note that $t_{1/2}$ and Q_{2h} for cases 4 and 5 (which are based on more reasonable thermal conductivity values) indicate much faster dissociation than what was observed in the laboratory experiment of case H5, providing further support to the earlier conclusion that the hydrate dissociation in case H5 could be a kinetic process.

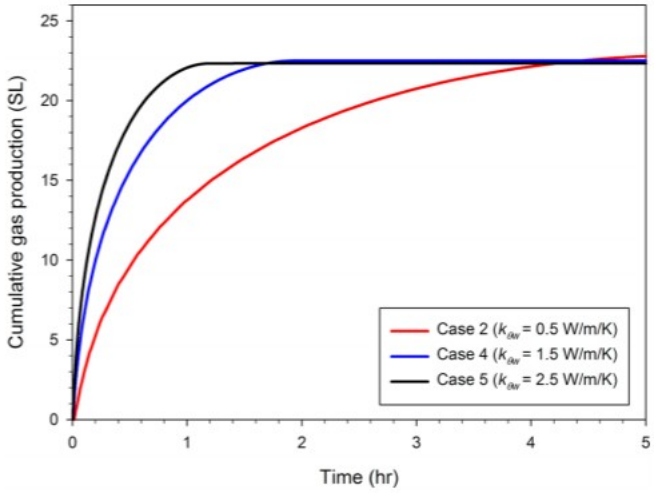

Figure 14. Cumulative gas production profile in cases 2, 4, and 5 with different sand wet thermal conductivities ($k_{\theta w}$).

Figure 15 plots the position of the hydrate dissociation front $X(t)$ against $t^{1/2}$ in cases 2, 4, and 5. A linear relationship is again identified and shown. The results in Figure 15 clearly show that the rate of advance of the hydrate dissociation front increases with an increasing $k_{\theta w}$ of the porous medium and confirm the earlier observations (Figure 14).

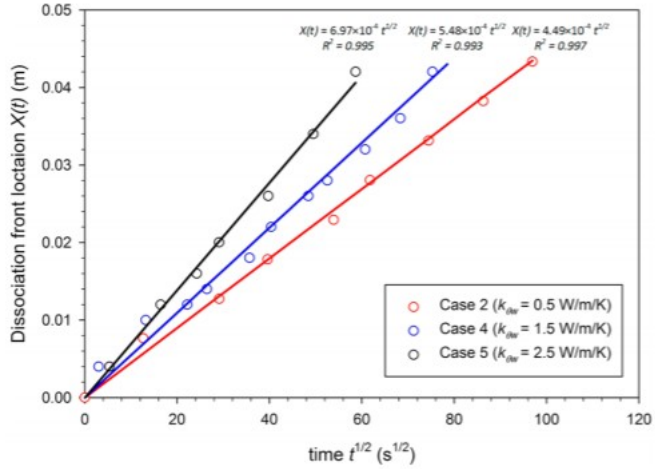

Figure 15. Location of hydrate dissociation front $X(t)$ against $t^{1/2}$ in cases 2, 4, and 5 with different sand wet thermal conductivities ($k_{\theta w}$).

3.5. Total Energy Consumption (Q_H) and Energy Efficiency Ratio

To evaluate the potential of gas production from hydrate reactor using thermal stimulation, we computed the total energy consumption for all simulated cases by monitoring the heat flow around the reactor boundary and then evaluated the overall energy efficiency ratio. The concept of EER in the context of gas production from hydrates was used by Selim and Sloan(28,31) and a number of hydrate dissociation experiments using various thermal stimulation techniques [e.g., huff and puff, steam-assisted gravity drainage (SAGD), and hot water flooding(10,77−81)]. EER is defined as the ratio of the energy content of the recovered CH_4 to the total heat input to the system shown in eq 1:(1)where V_T is the cumulative amount of methane produced and Q_H is the total amount of heat input; Q_C represents the heating value (heat of combustion) of CH_4 (3.97×10^7 J/m^3 CH_4 at STP(82)). V_T can be estimated from the simulation results, and Q_H can be calculated by integrating heat flow over time.

Table 5 summarizes the V_T and Q_H estimated from the simulation of the hydrate reactor experiments. The computed overall EER is in the range of 14.0–16.2. These values are higher than those reported by Selim and Sloan(28) (6.2–11.4), but these differences were expected because their analysis involved a very different system: a 1D hydrate-bearing sediment with $\phi = 0.3$ studied by using an analytical model. The results for cases 1, 2, and 3 indicate that higher $Q_H$is associated with higher boundary-wall

temperature, thus yielding a smaller EER value (as computed by eq 1). As expected, the value of composite thermal conductivity (cases 2, 4, and 5) has practically no effect on EER because Q_H is computed over the time to complete dissociation: the same total amount of energy is needed to effect full dissociation regardless of the rate of heat transport, hence the practical coincidence of the EER values.

Table 5. Estimated Total Gas Production (V_T), Total Energy Consumption (Q_H), and the Calculated EER for All Simulated Cases

simulated case	total gas production (SL)	total energy consumption (kJ)	EER
case 1	22.40	52.11	16.18
case 2 (base case)	22.84	57.75	14.89
case 3	22.92	61.57	14.01
case 4	22.51	57.75	14.67
case 5	22.51	57.75	14.67

4. Summary and Conclusion

In this study, we analyze numerically an earlier set of laboratory experiments of thermally induced hydrate dissociation in a sandy porous media in a 1.0 L hydrate reactor. We use the TOUGH+Hydrate v1.5 simulator and we describe the cylindrical reactor by a 2D axi-symmetric cylindrical mesh. Three simulated cases (cases 1, 2, and 3) describe the different thermal boundary temperatures used in the experimental studies. Two additional cases (cases 4 and 5) do not reproduce laboratory experiments but are sensitivity investigations designed to evaluate the effect of the “wet” thermal conductivity (i.e., when fully saturated with water) of sand ($k_{\theta w}$) on (a) the dynamic hydrate dissociation behavior and (b) on gas release and

production. There is a good agreement between the simulation results and the experimentally determined cumulative gas production over time.

The numerically computed spatial distributions of S_H, S_G, and S_A over time show that hydrate dissociates inward from the reactor boundary toward the inner core of the reactor and is characterized by a sharp hydrate dissociation front. Methane gas migrates to the outer shell of the reactor first and gradually accumulates at the upper section of the reactor because of buoyancy. A close examination on the location of the numerical prediction of the hydrate dissociation front $X(t)$ suggests a linear relationship with $t^{1/2}$. Sensitivity analysis indicates that the rate of hydrate dissociation increases with $k_{\theta w}$, which is in line with expectations because the conditions of the dissociation experiments are such that they are dominated by thermal (as opposed to flow) processes. Under the conditions of the thermally induced hydrate dissociation using boundary-wall heating of the experiments that we analyzed, the calculated overall EER values vary between 14.0 and 16.2, suggesting a high efficiency for energy recovery.

The numerical predictions of the rate of gas production and of the rate of advance of the dissociation front indicate faster dissociation than estimated in the laboratory experiments using different values of $k_{\theta w}$, and there is divergence between the measured and predicted evolution of temperature at the sensor locations. These deviations are attributed to three factors: (i) the assumption of uniformity in the initial hydrate saturation S_H, the validity of which cannot be ascertained without access to CT scanning; (ii) the assumption of dissociation as an equilibrium (as opposed to kinetic) reaction; and, to a lesser extent, (iii) uncertainty in the value of $k_{\theta w}$. The results tend to indicate that hydrate dissociation, as executed in the experiments, was a kinetic process.

The main conclusions that are drawn from this study are as follows:

(a) Knowledge of the initial spatial distributions and heterogeneity of the various phase saturations in hydrate-bearing media is an important (and possibly critical) input in the analysis of hydrate dissociation experiments. If it is not possible to determine experimentally these distributions (e.g., by using a CT scanning process), then, at a minimum, numerically predicted distributions should be used. These will need to accurately reflect the controlled laboratory conditions under which the artificial hydrate samples had been synthesized. We plan to follow this process in a future analysis the laboratory study analyzed here.(1)

(b) The numerical predictions based on the assumption that hydrate dissociation is described by an equilibrium reaction lead to faster dissociation than what has been observed in laboratory experiments. Sensitivity analysis indicates that this cannot be explained only by the thermal conductivity value, thus providing evidence of kinetic retardation. This appears to be consistent with earlier observations(23) that kinetic behavior is important in short-term processes such as laboratory experiments and needs to be

considered in their analysis. In a future study, we plan to thoroughly explore the issue.

Acknowledgments

The financial support from the National University of Singapore (R-261-508-001-646/733) is greatly appreciated. Z.Y. thanks the EDB industrial postgraduate programme (IPP) for the scholarship. G.M. thanks ExxonMobil and NUS for the ExxonMobil Visiting Chair position in the Department of Chemical and Biomolecular Engineering at NUS.

Symbols

A	aqueous phase
C_R	heat capacity of rock (J/kg/K)
EER	energy efficiency ratio
G	gas phase
GRR	gas recovery ratio
H	hydrate phase
k	intrinsic permeability (m^2)
k_{rA}	relative permeability of aqueous phase
k_{rG}	relative permeability of gas phase
k_θ	composite thermal conductivity of hydrate bearing sediment (W/m/K)
$k_{\theta d}$	thermal conductivity of dry porous medium (W/m/K)
$k_{\theta w}$	thermal conductivity of fully saturated porous medium (W/m/K)
n_A, n_G	parameters in modified Stone's model for relative permeability
N_H	hydration number
P	pressure (Pa)
P_0	air entry pressure (Pa)
P_{cap}	capillary pressure (Pa)
Q_C	heat of combustion of methane gas (J/m^3)
Q_H	total heat supply to the hydrate reactor (J)
STP	standard temperature and pressure (273 K and 1 atm)
S^*	effective water saturation

t time (s)

T temperature (K)

ΔT temperature differential (K)

V_T cumulative gas production at time (SL)

$X(t)$ hydrate dissociation front location as a function of time (m)

Δr discretization along the r axis (mm)

Δz discretization along the z axis (mm)

ΔH^0 associated enthalpy due to hydrate dissociation (kJ/mol)

Subscripts and Superscripts

A aqueous phase

cap Capillary

eq equilibrium conditions

G gas phase

H hydrate phase

i_{rA} irreducible aqueous phase

i_{rG} irreducible gas phase

I ice phase

L_w liquid water phase

M methane component

R Rock

W water component

Greek Letters

ρ density (kg/m^3)

ϕ Porosity

ξ nondimensional parameter for hydrate dissociation location

λ parameter in the capillary pressure model of van Genuchten

References

1. Chong, Z. R.; Pujar, G. A.; Yang, M.; Linga, P. Methane Hydrate Formation in Excess Water Simulating Marine Locations and the Impact of Thermal Stimulation on Energy Recovery. *Appl. Energy* 2016, *177*,409– 421, DOI: 10.1016/j.apenergy.2016.05.077

2. Chong, Z. R.; Yang, S. H. B.; Babu, P.; Linga, P.; Li, X.-S. Review of Natural Gas Hydrates as an Energy Resource: Prospects and Challenges. *Appl. Energy* 2016, *162*, 1633– 1652, DOI: 10.1016/j.apenergy.2014.12.061

3. Moridis, G. J.; Collett, T. S.; Boswell, R.; Kurihara, M.; Reagan, M. T.; Koh, C.; Sloan, E. D. Toward Production from Gas hydrates: Current Status, Assessment of Resources, and Simulation-based Evaluation of Technology and Potential. *SPE Reservoir Eval. Eng.* 2009, *12* (5), 745– 771, DOI: 10.2118/114163-PA

4. Boswell, R.; Collett, T. S. Current Perspectives on Gas Hydrate Resources. *Energy Environ. Sci.* 2011, *4* (4),1206– 1215, DOI: 10.1039/C0EE00203H

5. Sloan, E. D., Jr.; Koh, C. A. *Clathrate Hydrates of Natural Gases*, 3rd ed.; CRC Press: Boca Raton, FL,2008.

6. Collett, T. S. Energy Resource Potential of Natural Gas Hydrates. *AAPG Bull.* 2002, *86* (11), 1971– 1992,DOI: 10.1306/61EEDDD2-173E-11D7-8645000102C1865D

7. Collett, T.; Bahk, J.-J.; Frye, M.; Goldberg, D.; Husebo, J.; Koh, C.; Malone, M.; Shipp, C.; Torres, M.*Historical Methane Hydrate Project Review*; Consortium for Ocean Leadership: Washington, DC, 2013.

8. Moridis, G. J.; Collett, T. S.; Pooladi-Darvish, M.; Hancock, S. H.; Santamarina, J. C.; Boswell, R.;Kneafsey, T. J.; Rutqvist, J.; Reagan, M. T.; Sloan, E. D.; Sum, A.; Koh, C. Challenges, Uncertainties, and Issues Facing Gas Production from Gas-hydrate Deposits. *SPE Reservoir Eval. Eng.* 2011, *14*, 76– 112,DOI: 10.2118/131792-PA

9. Linga, P.; Haligva, C.; Nam, S. C.; Ripmeester, J. A.; Englezos, P. Recovery of Methane from Hydrate Formed in a Variable Volume Bed of Silica Sand Particles. *Energy Fuels* 2009, *23* (11), 5508– 5516, DOI: 10.1021/ef900543v

10. Li, X.-S.; Wang, Y.; Li, G.; Zhang, Y. Experimental Investigations into Gas Production Behaviors from Methane Hydrate with Different Methods in a Cubic Hydrate Simulator. *Energy Fuels* 2012, *26* (2), 1124–1134, DOI: 10.1021/ef201641v

11. Makogon, Y. F. *Hydrates of Hydrocarbons*; Pennwell Books: Tulsa, OK, 1997.

12. Ohgaki, K.; Takano, K.; Sangawa, H.; Matsubara, T.; Nakano, S. Methane Exploitation by Carbon Dioxide from Gas Hydrates. Phase Equilibria for CO_2-CH_4 Mixed Hydrate System. *J. Chem. Eng. Jpn.* 1996, *29* (3),478– 483, DOI: 10.1252/jcej.29.478

13. Kvamme, B.; Graue, A.; Buanes, T.; Kuznetsova, T.; Ersland, G. Storage of CO_2 in Natural Gas Hydrate Reservoirs and the Effect of Hydrate as an Extra Sealing in Cold Aquifers. *Int. J. Greenhouse Gas Control*2007, *1* (2), 236– 246, DOI: 10.1016/S1750-5836(06)00002-8

14. Anderson, B.; Boswell, R.; Collett, T. S.; Farrell, H.; Ohtsuki, S.; White, M.; Zyrianova, M. Review of the Findings of the Iġnick Sikumi CO_2–CH_4 Gas Hydrate Exchange Field Trial. In *Proceedings of the 8th International Conference on Gas Hydrates*, Beijing, 2014.

15. Alp, D.; Parlaktuna, M.; Moridis, G. J. Gas Production by Depressurization from Hypothetical Class 1G and Class 1W Hydrate Reservoirs. *Energy Convers. Manage.* 2007, *48* (6), 1864– 1879, DOI: 10.1016/j.enconman.2007.01.009

16. Moridis, G. J.; Kowalsky, M. B.; Pruess, K. Depressurization-induced Gas Production from Class-1 Hydrate Deposits. *SPE Reservoir Eval. Eng.* 2007, *10* (05), 458– 481, DOI: 10.2118/97266-PA

17. Moridis, G. J.; Reagan, M. T. Strategies for Gas Production from Oceanic Class 3 Hydrate Accumulations. In Offshore Technology Conference, Houston, TX, April 30–May 3, 2007; Offshore Technology Conference: OTC, 2007.

18. Moridis, G. J.; Silpngarmlert, S.; Reagan, M. T.; Collett, T.; Zhang, K. Gas Production from a Cold, Stratigraphically-bounded Gas Hydrate Deposit at the Mount Elbert Gas Hydrate Stratigraphic Test Well, Alaska North Slope: Implications of Uncertainties. *Mar. Pet. Geol.* 2011, *28* (2), 517– 534, DOI: 10.1016/j.marpetgeo.2010.01.005

19. Reagan, M. T.; Moridis, G. J.; Johnson, J. N.; Pan, L.; Freeman, C. M.; Boyle, K. L.; Keen, N. D.; Husebo, J.Field-scale Simulation of Production from Oceanic Gas Hydrate Deposits. *Transp. Porous Media* 2015, *108*(1), 151–169, DOI: 10.1007/s11242-014-0330-7

20. Moridis, G. J.; Kim, J.; Reagan, M. T.; Kim, S.-J. Feasibility of Gas Production from a Gas Hydrate Accumulation at the UBGH2–6 Site of the Ulleung Basin in the Korean East Sea. *J. Pet. Sci. Eng.* 2013,*108*, 180– 210, DOI: 10.1016/j.petrol.2013.03.002

21. Moridis, G. J.; Reagan, M. T. Estimating the Upper Limit of Gas Production from Class 2 Hydrate Accumulations in the Permafrost: 2. Alternative Well Designs and Sensitivity Analysis. *J. Pet. Sci. Eng.*2011, *76* (3), 124– 137, DOI: 10.1016/j.petrol.2010.12.001

22. Moridis, G. J.; Reagan, M. T. Estimating the Upper limit of Gas Production from Class 2 Hydrate Accumulations in the Permafrost: 1. Concepts, System Description, and the Production Base Case. *J. Pet. Sci. Eng.* 2011, *76* (3), 194– 204, DOI: 10.1016/j.petrol.2010.11.023

23. Kowalsky, M. B.; Moridis, G. J. Comparison of Kinetic and Equilibrium Reaction Models in Simulating Gas Hydrate Behavior in Porous Media. *Energy Convers. Manage.* 2007, *48* (6), 1850– 1863, DOI: 10.1016/j.enconman.2007.01.017

24. Moridis, G. J.; Sloan, E. D. Gas Production Potential of Disperse Low-saturation Hydrate Accumulations in Oceanic Sediments. *Energy Convers. Manage.* 2007, *48* (6), 1834– 1849, DOI: 10.1016/j.enconman.2007.01.023

25. Moridis, G. J.; Reagan, M. T.; Boyle, K. L.; Zhang, K. Evaluation of the Gas Production Potential of Some Particularly Challenging Types of Oceanic Hydrate Deposits. *Transp. Porous Media* 2011, *90* (1), 269– 299,DOI: 10.1007/s11242-011-9762-5

26. Yin, Z.; Chong, Z. R.; Tan, H. K.; Linga, P. Review of Gas Hydrate Dissociation Kinetic Models for Energy Recovery. *J. Nat. Gas Sci. Eng.* 2016, *35*, 1362– 1387, DOI: 10.1016/j.jngse.2016.04.050

27. Kim, H. C.; Bishnoi, P. R.; Heidemann, R. A.; Rizvi, S. S. H. Kinetics of Methane Hydrate Decomposition.*Chem. Eng. Sci.* 1987, *42* (7), 1645– 1653, DOI: 10.1016/0009-2509(87)80169-0

28. Selim, M.; Sloan, E. Heat and Mass Transfer during the Dissociation of Hydrates in Porous Media. *AIChE J.*1989, *35* (6), 1049– 1052, DOI: 10.1002/aic.690350620

29. Yousif, M.; Abass, H.; Selim, M.; Sloan, E. Experimental and Theoretical Investigation of Methane-gas-hydrate Dissociation in Porous Media. *SPE Reservoir Eng.* 1991, *6* (01), 69– 76, DOI: 10.2118/18320-PA

30. Clarke, M.; Bishnoi, P. R. Determination of the Intrinsic Rate of Gas Hydrate Decomposition using Particle Size Analysis. *Ann. N. Y. Acad. Sci.* 2000, *912* (1), 556– 563, DOI: 10.1111/j.1749-6632.2000.tb06810.x

31. Selim, M. S.; Sloan, E. D. Modeling of the Dissociation of an In-situ Hydrate. In SPE California Regional Meeting, Society of Petroleum Engineers: Bakersfield, CA, 1985; pp 75– 80.

32. Ahmadi, G.; Ji, C.; Smith, D. H. Numerical Solution for Natural Gas Production from Methane Hydrate Dissociation. *J. Pet. Sci. Eng.* 2004, *41* (4), 269– 285, DOI: 10.1016/j.profnurs.2003.09.004

33. Nazridoust, K.; Ahmadi, G. Computational Modeling of Methane Hydrate Dissociation in a Sandstone Core.*Chem. Eng. Sci.* 2007, *62* (22), 6155– 6177, DOI: 10.1016/j.ces.2007.06.038

34. Sun, X.; Mohanty, K. K. Kinetic Simulation of Methane Hydrate Formation and Dissociation in Porous MSedia. *Chem. Eng. Sci.* 2006, *61* (11), 3476– 3495, DOI: 10.1016/j.ces.2005.12.017

35. Moridis, G. J. *User's manual for the hydrate v1. 5 option of TOUGH+ v1. 5: A code for the simulation of system behavior in hydrate-bearing geologic media*; LBNL 6869E; Lawrence Berkeley National Laboratory:Berkeley, CA, 2014.

36. Moridis, G. *User's manual of the TOUGH+ core code v1. 5: A general-purpose simulator of non-isothermal flow and transport through porous and fractured media*; LBNL 6871E; Lawrence Berkeley National Laboratory: Berkeley, CA, 2014.

37. Moridis, G.; Apps, J.; Pruess, K.; Myer, L. *EOSHYDR: A TOUGH2 Module for CH_4-hydrate Release and Flow in the Subsurface*; LBNL 42386; Lawrence Berkeley National Laboratory: Berkeley, CA, 1998.

38. Moridis, G. Numerical Studies of Gas Production from Methane Hydrates. *SPE J.* 2003, *8* (4), 359– 370,DOI: 10.2118/87330-PA

39. Moridis, G. J.; Collett, T. S.; Dallimore, S. R.; Satoh, T.; Hancock, S.; Weatherill, B. Numerical Studies of Gas Production from Several CH_4 Hydrate Zones at the Mallik Site, Mackenzie Delta, Canada. *J. Pet. Sci. Eng.* 2004, *43* (3), 219– 238, DOI: 10.1016/j.petrol.2004.02.015

40. Moridis, G. J.; Collett, T. S. Gas Production from Class 1 Hydrate Accumulations. In *Advances in the Study of Gas Hydrates*; Springer: New York, 2004; pp 83– 97.

41. Moridis, G.; Kowalsky, M.; Pruess, K. *TOUGH-Fx/HYDRATE v1. 0.1 user's manual: A code for the simulation of system behavior in hydratebearing geologic media*; LBNL 3185; Lawrence Berkeley National Laboratory: Berkeley, CA, 2005.

42. Gamwo, I. K.; Liu, Y. Mathematical Modeling and Numerical Simulation of Methane Production in a Hydrate Reservoir. *Ind. Eng. Chem. Res.* 2010, *49* (11), 5231– 5245, DOI: 10.1021/ie901452v

43. Kurihara, M.; Sato, A.; Ouchi, H.; Narita, H.; Masuda, Y.; Saeki, T.; Fujii, T. Prediction of Gas Productivity from Eastern Nankai Trough Methane-hydrate Reservoirs. In *Offshore Technology Conference*, Houston, TX, 2008; Vol. OTC-19382-MS.

44. White, M. D. *STOMP-HYDT-KE A Numerical Simulator for the Production of Natural Gas Hydrate using Guest Molecule Exchange with CO_2 and N_2*; PNNL-22130; Pacific Northwest National Laboratory: Richland, WA, 2006.

45. Uddin, M.; Coombe, D.; Law, D.; Gunter, B. Numerical Studies of Gas Hydrate Formation and Decomposition in a Geological Reservoir. *J. Energy Resour. Technol.* 2008, *130* (3), 032501, DOI: 10.1115/1.2956978

46. Hong, H.; Pooladi-Darvish, M. Simulation of Depressurization for Gas Production from Gas Hydrate Reservoirs. *J. Can. Pet. Technol.* 2005, 44, (11). DOI: DOI: 10.2118/05-11-03 .

47. Wilder, J. W.; Moridis, G. J.; Wilson, S. J.; Kurihara, M.; White, M. D.; Masuda, Y.; Anderson, B.;Collett, T. S.; Hunter, R.; Narita, H.; Pooladi-Darvish, M.; Rose, K.; Boswell, R. An International Effort to Compare Gas Hydrate Reservoir Simulators. In 6th International Conference on Gas Hydrates, Vancouver, Canada, 2008.

48. Li, B.; Li, X.-S.; Li, G.; Feng, J.-C.; Wang, Y. Depressurization Induced Gas Production from Hydrate Deposits with Low Gas Saturation in a Pilot-scale Hydrate Simulator. *Appl. Energy* 2014, *129*, 274– 286,DOI: 10.1016/j.apenergy.2014.05.018

49. Liang, H.; Song, Y.; Chen, Y. Numerical Simulation for Laboratory-scale Methane Hydrate Dissociation by Depressurization. *Energy Convers. Manage.* 2010, *51* (10), 1883– 1890, DOI: 10.1016/j.enconman.2010.02.018

50. Linga, P.; Haligva, C.; Nam, S. C.; Ripmeester, J. A.; Englezos, P. Gas Hydrate Formation in a Variable Volume Bed of Silica Sand Particles. *Energy Fuels* 2009, *23* (11), 5496– 5507, DOI: 10.1021/ef900542m

51. Li, B.; Li, G.; Li, X.-S.; Li, Q.-P.; Yang, B.; Zhang, Y.; Chen, Z.-Y. Gas Production from Methane Hydrate in a Pilot-scale Hydrate Simulator using the Huff and Puff Method by Experimental and Numerical Studies.*Energy Fuels* 2012, *26* (12), 7183– 7194, DOI: 10.1021/ef301258w

52. Kneafsey, T. J.; Tomutsa, L.; Moridis, G. J.; Seol, Y.; Freifeld, B. M.; Taylor, C. E.; Gupta, A. Methane Hydrate Formation and Dissociation in a Partially Saturated Core-scale Sand Sample. *J. Pet. Sci. Eng.*2007, *56* (1), 108– 126, DOI: 10.1016/j.petrol.2006.02.002

53. Moridis, G. J.; Seol, Y.; Kneafsey, T. J. Studies of Reaction Kinetics of Methane Hydrate Dissocation in Porous Media. In 5th International Conference on gas Hydrates, Trondheim, Norway, June 13–16, 2005; pp21–30.

54. Gupta, A.; Kneafsey, T. J.; Moridis, G. J.; Seol, Y.; Kowalsky, M. B.; Sloan, E. Composite Thermal Conductivity in a Large Heterogeneous Porous Methane Hydrate Sample. *J. Phys. Chem. B* 2006, *110* (33),16384– 16392, DOI: 10.1021/jp0619639

55. Kamath, V. A. Study of Heat Transfer Characteristics during Dissociation of Gas Hydrates in Porous Media. Ph.D. Thesis, University of Pittsburgh, Pittsburgh, PA, 1983.

56. Liu, Y.; Gamwo, I. K. Comparison between Equilibrium and Kinetic Models for Methane Hydrate Dissociation. *Chem. Eng. Sci.* 2012, *69* (1), 193– 200, DOI: 10.1016/j.ces.2011.10.020

57. Bagherzadeh, S. A.; Moudrakovski, I. L.; Ripmeester, J. A.; Englezos, P. Magnetic Resonance Imaging of Gas Hydrate Formation in a Bed of Silica Sand Particles. *Energy Fuels* 2011, *25* (7), 3083– 3092, DOI: 10.1021/ef200399a

58. Moridis, G. *User's nannual of the MeshMaker v1. 5 code: A mesh generator for domain discretization in simulations of the TOUGH+ and TOUGH2 familes of codes*; LBNL 1005134; Lawrence Berkeley National Laboratory: Berkeley, CA, 2016.

59. Stone, H. Probability Model for Estimating Three-phase Relative Permeability. *JPT, J. Pet. Technol.* 1970,*22* (02), 214– 218, DOI: 10.2118/2116-PA

60. Ghanbarian-Alavijeh, B.; Liaghat, A.; Huang, G.-H.; Van Genuchten, M. T. Estimation of the van Genuchten Soil Water Retention Properties from Soil

Textural Data. *Pedosphere* 2010, *20* (4), 456– 465, DOI: 10.1016/S1002-0160(10)60035-5

61. Van Genuchten, M. T. A Closed-form Equation for Predicting the Hydraulic Conductivity of Unsaturated Soils. *Soil Sci. Soc. Am. J.* 1980, *44* (5), 892–898, DOI: 10.2136/sssaj1980.03615995004400050002x

62. Kamath, V. A.; Godbole, S. P. Evaluation of Hot-brine Stimulation Technique for Gas Production from Natural Gas Hydrates. *JPT, J. Pet. Technol.* 1987, *39* (11), 1379– 1388, DOI: 10.2118/13596-PA

63. Côté, J.; Konrad, J.-M. A Generalized Thermal Conductivity Model for Soils and Construction Materials.*Can. Geotech. J.* 2005, *42* (2), 443– 458, DOI: 10.1139/t04-106

64. Zhang, N.; Yu, X.; Pradhan, A.; Puppala, A. J. Thermal Conductivity of Quartz Sands by Thermo-time Domain Reflectometry Probe and Model Prediction. *J. Mater. Civ. Eng.* 2015, *27* (12), 04015059, DOI: 10.1061/(ASCE)MT.1943-5533.0001332

65. Tarnawski, V. R.; Leong, W. H. Advanced Geometric Mean model for Predicting Thermal Conductivity of Unsaturated Soils. *Int. J. Thermophys.* 2016, *37* (2), 18, DOI: 10.1007/s10765-015-2024-y

66. Tarnawski, V. R.; Momose, T.; Leong, W. H. Thermal Conductivity of Standard Sands II. Saturated Conditions. *Int. J. Thermophys.* 2011, *32* (5), 984, DOI: 10.1007/s10765-011-0975-1

67. Hu, H.; Argyropoulos, S. A. Mathematical Modelling of Solidification and Melting: A Review. *Modell. Simul. Mater. Sci. Eng.* 1996, *4* (4), 371, DOI: 10.1088/0965-0393/4/4/004

68. Paterson, S. Propagation of a Boundary of Fusion. *Glasgow Math. J.* 1952, *1* (1), 42– 47, DOI: 10.1017/S2040618500032937

69. Rosenbaum, E. J.; English, N. J.; Johnson, J. K.; Shaw, D. W.; Warzinski, R. P. Thermal Conductivity of Methane Hydrate from Experiment and Molecular Simulation. *J. Phys. Chem. B* 2007, *111* (46), 13194–13205, DOI: 10.1021/jp074419o

70. Ji, C.; Ahmadi, G.; Smith, D. H. Natural Gas Production from Hydrate Decomposition by Depressurization.*Chem. Eng. Sci.* 2001, *56* (20), 5801–5814, DOI: 10.1016/S0009-2509(01)00265-2

71. Chuvilin, E.; Bukhanov, B. Effect of Hydrate Formation Conditions on Thermal Conductivity of Gas-saturated Sediments. *Energy Fuels* 2017, *31* (5), 5246– 5254, DOI: 10.1021/acs.energyfuels.6b02726

72. Krinsley, D. H.; Doornkamp, J. C. *Atlas of Quartz Sand Surface Textures*; Cambridge University Press:Cambridge, 2011.

73. Bagherzadeh, S. A.; Alavi, S.; Ripmeester, J.; Englezos, P. Formation of Methane Nano-bubbles during Hydrate Decomposition and Their Effect on

Hydrate Growth. *J. Chem. Phys.* 2015, *142* (21), 214701, DOI: 10.1063/1.4920971

74. Bagherzadeh, S. A.; Englezos, P.; Alavi, S.; Ripmeester, J. A. Molecular Simulation of Non-equilibrium Methane Hydrate Decomposition Process. *J. Chem. Thermodyn.* 2012, *44* (1), 13– 19, DOI: 10.1016/j.jct.2011.08.021

75. Bagherzadeh, S. A.; Englezos, P.; Alavi, S.; Ripmeester, J. A. Molecular Modeling of the Dissociation of Methane Hydrate in Contact with a Silica Surface. *J. Phys. Chem. B* 2012, *116* (10), 3188– 3197, DOI: 10.1021/jp2086544

76. Clauser, C.; Huenges, E. Thermal Conductivity of Rocks and Minerals. *Rock physics & phase relations: A handbook of physical constants* 1995, *3*, 105– 126, DOI: 10.1029/RF003p0105

77. Feng, J.-C.; Wang, Y.; Li, X.-S.; Li, G.; Zhang, Y.; Chen, Z.-Y. Effect of Horizontal and Vertical Well Patterns on Methane Hydrate Dissociation Behaviors in Pilot-scale Hydrate Simulator. *Appl. Energy* 2015, *145*, 69–79, DOI: 10.1016/j.apenergy.2015.01.137

78. Tang, L. G.; Xiao, R.; Huang, C.; Feng, Z.; Fan, S. S. Experimental Investigation of Production Behavior of Gas Hydrate under Thermal Stimulation in Unconsolidated Sediment. *Energy Fuels* 2005, *19* (6), 2402–2407, DOI: 10.1021/ef050223g

79. Li, G.; Li, X.-S.; Yang, B.; Duan, L.-P.; Huang, N.-S.; Zhang, Y.; Tang, L.-G. The Use of Dual Horizontal Wells in Gas Production from Hydrate Accumulations. *Appl. Energy* 2013, *112*, 1303– 1310, DOI: 10.1016/j.apenergy.2013.03.057

80. Li, X.-S.; Yang, B.; Duan, L.-P.; Li, G.; Huang, N.-S.; Zhang, Y. Experimental Study on Gas Production from Methane Hydrate in Porous Media by SAGD Method. *Appl. Energy* 2013, *112*, 1233– 1240, DOI: 10.1016/j.apenergy.2013.02.007

81. Li, G.; Li, X.-S.; Li, B.; Wang, Y. Methane Hydrate Dissociation using Inverted Five-spot Water Flooding Method in Cubic Hydrate Simulator. *Energy* 2014, *64*, 298– 306, DOI: 10.1016/j.energy.2013.10.015

82. Pittam, D. A.; Pilcher, G. Measurements of Heats of Combustion by Flame Calorimetry. Part 8.-Methane, Ethane, Propane, N-butane and 2-methylpropane. *J. Chem. Soc., Faraday Trans. 1* 1972, *68* (0), 2224–2229, DOI: 10.1039/f19726802224